nature publishing group

Intrinsic cardiomyopathy in Marfan syndrome: results from *in-vivo* and *ex-vivo* studies of the *Fbn1*$^{C1039G/+}$ model and longitudinal findings in humans

Laurence Campens[1], Marjolijn Renard[1], Bram Trachet[2], Patrick Segers[2], Laura Muino Mosquera[1], Johan De Sutter[3], Lynn Sakai[4], Anne De Paepe[1] and Julie De Backer[1]

BACKGROUND: Mild intrinsic cardiomyopathy in patients with Marfan syndrome (MFS) has consistently been evidenced by independent research groups. So far, little is known about the long-term evolution and pathophysiology of this finding.

METHODS: To gain more insights into the pathophysiology of MFS-related cardiomyopathy, we performed *in-vivo* and *ex-vivo* studies of 11 *Fbn1*$^{C1039G/+}$ mice and 9 wild-type (WT) littermates. Serial ultrasound findings obtained in mice were correlated to the human phenotype. We therefore reassessed left ventricular (LV) function parameters over a 6-y follow-up period in 19 previously reported MFS patients, in whom we documented mild LV dysfunction.

RESULTS: *Fbn1*$^{C1039G/+}$ mice demonstrated LV contractile dysfunction. Subsequent *ex-vivo* studies of the myocardium of adult mutant mice revealed upregulation of TGFβ-related pathways and consistent abnormalities of the microfibrillar network, implicating a role for microfibrils in the mechanical properties of the myocardium. Echocardiographic parameters did not indicate clinical significant deterioration of LV function during follow-up in our patient cohort.

CONCLUSION: In analogy with what is observed in the majority of MFS patients, the *Fbn1*$^{C1039G/+}$ mouse model demonstrates mild intrinsic LV dysfunction. Both extracellular matrix and molecular alterations are implicated in MFS-related cardiomyopathy. This model may now enable us to study therapeutic interventions on the myocardium in MFS.

Marfan syndrome (MFS, GenBank accession nos. ***L13923***) is an autosomal dominant inherited connective tissue disorder caused by mutations in the *fibrillin-1* gene (*FBN1*) encoding the extracellular matrix protein fibrillin-1. The clinical diagnosis of MFS relies on the identification of characteristic clinical manifestations, mainly occurring in the cardiovascular, musculoskeletal, and ocular system, as summarized in the "Revised Ghent Nosology", and may be supplemented by the identification of a causal *FBN1* mutation (1).

Cardiovascular involvement in MFS is characterized by progressive dilatation of the ascending aorta at the level of the sinuses of Valsalva, ensuing a risk for type A aortic dissection or -rupture and aortic valve regurgitation (2). Other established cardiovascular manifestations of MFS include mitral valve prolapse and pulmonary artery dilatation. More recently, several independent studies demonstrated the presence of—mostly subclinical—intrinsic cardiomyopathy (CMP) with both left and right ventricular (LV and RV) systolic and diastolic dysfunction in MFS patients (3,4). The current knowledge of MFS-related CMP is based on cross-sectional studies, but little is known about the long-term evolution and pathophysiology of this finding.

To unravel the underlying pathophysiology of MFS-related CMP, the knowledge obtained from the study of other MFS manifestations may at least be partly translated to the cardiac phenotype. Upregulation of TGFβ signaling, with activation of the canonical (SMAD2/3) and noncanonical (predominantly ERK1/2) pathways, is implicated in aortic dilatation, mitral valve prolapse, pulmonary emphysema, and skeletal myopathy (reviewed in ref. (5)). Interestingly, TGFβ upregulation has been evidenced in hereditary CMP (dilated, hypertrophic, and arrhythmogenic right ventricular CMP), where it is linked to cardiac interstitial fibrosis (6–10). In the *Fbn1*$^{mgR/mgR}$ model, which is a severe murine model for MFS demonstrating dilated CMP from 2 mo of age, selective upregulation of the noncanonical signaling pathway was evidenced (11). In addition to its role as a regulator of TGFβ bioavailability, fibrillin-1 has an important structural role, providing stability and elasticity to tissues. Structural dysfunction is implicated in several MFS manifestations including lens luxation and aortic dilatation (12). Additionally, loss of mechanical properties of the microfibrillar network in the myocardium may evoke ventricular dysfunction (11–13). Another mechanism through which aberrant microfibrils could lead to contractile dysfunction of the myocardium, is through loss of binding to integrin receptors, which play a key role in cell-matrix interactions (extracellular matrix (ECM)) and mechanotransduction

[1]Center for Medical Genetics Ghent, Ghent University Hospital, Ghent, Belgium; [2]IBiTech-bioMMeda, Ghent University, Ghent, Belgium; [3]Internal Medicine, Ghent University, Ghent, Belgium; [4]Shriners Hospital for Children, Oregon Health & Science University, Portland, Oregon. Correspondence: Laurence Campens (Laurence.campens@ugent.be)

Received 16 November 2014; accepted 3 March 2015; advance online publication 1 July 2015. doi:10.1038/pr.2015.110

across the cell surface through the cytoskeleton (14–16). This hypothesis is supported by the observation that disruption of the integrin pathway leads to the development of CMP in both mice and humans (17–19). Interestingly, the downstream integrin pathway is downregulated in the myocardium of the *Fbn1*$^{mgR/mgR}$ model (11).

The objective of the current study is to gain more insight into the underlying pathophysiology of MFS-related CMP. To this aim, we first performed longitudinal ultrasound studies using a representative and well-characterized murine model for MFS, the *Fbn1*$^{C1039G/+}$ model, and compared our findings to the human cardiac phenotype. Subsequently, we explored structural and molecular alterations in the mouse myocardium.

RESULTS

Serial Ultrasound Data in the *Fbn1*$^{C1039G/+}$ Mouse Model

Although there was a nonsignificant trend toward larger aortic diameters at 1 and 3 mo, aortic diameters in the *Fbn1*$^{C1039G/+}$ mice were only significantly increased from month 6 onward when compared to wild-type (WT) mice. Aortic dilatation extended from the sinuses of Valsalva to the ascending and transverse aorta (**Table 1**)—which is different from the human aortic phenotype being limited to the level of the aortic sinus in most cases. Main pulmonary artery diameters were not significantly different between both groups. During follow-up, two MFS mice died of aortic dissection at 47 and 48 wk of age; on their scan at 6 mo they exhibited severe aortic dilatation associated with significant aortic valve regurgitation. At the end of the follow-up period, three additional MFS mice had developed significant aortic valve regurgitation with holodiastolic flow reversal in the descending aorta; in one of them this was already apparent on the scan at 6 mo. None of the WT mice presented significant aortic valve dysfunction. After 12 mo, two additional MFS mice died, one of dissection at 60 wk, the other died shortly after the last scan and demonstrated no evidence for aortic dissection or internal hemorrhage on necropsy.

LV fractional shortening was lower in MFS mice at all time points with significantly lower values at 6 mo (30.9% ± 7.9) vs. 41.2% ± 3.0; P = 0.001) (**Figure 1**). From 6 mo onward, fractional shortening remained stable (31.6% ± 5.5 at 12 mo, P = 0.71). Heart rate, weight, sex, sinus diameter, and aortic regurgitation were not identified as confounding factors of LV fractional shortening with univariate regression analysis (P = 0.61, P = 0.99, P = 0.53, P = 0.68, and P = 0.81, respectively).

We found no differences in diastolic function between MFS and WT mice (**Table 1**).

Table 1. Echocardiographic parameters of *Fbn1*$^{C1039G/+}$ mice at 12 mo of age

	WT	MFS	
	N = 9	N = 9	P value
Females	4 (44%)	6 (66%)	0.64
Weight (kg)	27.7 ± 3.4	26.2 ± 4.7	0.34
HR (bpm)	423.8 ± 19.1	425.8 ± 27.0	0.95
Aortic diameters			
Sinus (mm)	1.9 ± 0.2	2.6 ± 0.5	0.003
Ascending aorta (mm)	1.7 ± 0.2	2.3 ± 0.7	0.014
Arch (mm)	1.4 ± 0.1	1.8 ± 0.2	0.006
Descending aorta (mm)	1.2 ± 0.1	1.3 ± 0.2	0.014
Main pulmonary artery (mm)	1.4 ± 0.2	1.6 ± 0.3	0.38
LVEDD (mm)	3.7 ± 0.4	3.7 ± 0.7	1.0
LVESD (mm)	2.1 ± 0.2	2.5 ± 0.5	0.063
FS (%)	42.0 ± 6.3	31.6 ± 5.5	0.011
E/A	1.4 ± 0.4	1.1 ± 0.2	0.14
DT (ms)	14.9 ± 3.7	17.7 ± 7.1	0.74
E_m (mm/s)	21.4 ± 8.2	23.9 ± 11.1	0.73
E/E_m	37.1 ± 23.7	23.4 ± 5.8	0.20

DT, deceleration time; FS, fractional shortening; HR, heart rate; LVEDD, left ventricular end diastolic diameter; LVESD, left ventricular end systolic diameter; MFS, Marfan syndrome; WT, wild type.

Clinical Studies

Impaired ventricular function has been established in humans (3,4), but so far, no data on evolutionary changes have been reported. In view of our results obtained in mice, we aimed to provide longitudinal human data for which we analyzed echocardiographic studies at different time-points available from our MFS patient population. An initial detailed study of left ventricular function in this population indicated mild intrinsic LV systolic and diastolic dysfunction (20). Data obtained from the subsequent preliminary retrospective analysis demonstrate stable LV dimensions and no clinically significant decline of LV systolic or diastolic function (**Table 2**). Two patients developed moderate valvular dysfunction upon follow-up (one patient with aortic and one with mitral valve dysfunction)

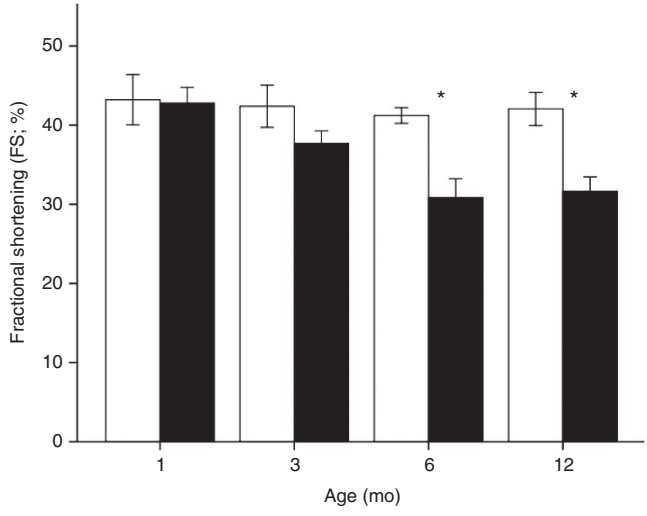

Figure 1. Bar chart with error bars (representing 1 standard error) of left ventricular fractional shortening of 11 *Fbn1*$^{C1039G/+}$ and 9 wild-type (WT) mice at 1, 3, and 6 mo and in 9 *Fbn1*$^{C1039G/+}$ and 9 WT mice at 12 mo of age. *Fbn1*$^{C1039G/+}$ mice demonstrate significant lower fractional shortening from 6 mo of age on in comparison to WT mice. White bars represent WT mice and black bars *Fbn1*$^{C1039G/+}$ mice. FS, fractional shortening (%).*P value < 0.05.

Table 2. Systolic and diastolic function parameters of MFS patients and sex- and age-matched controls at baseline (T_0) and of the MFS cohort after follow-up (T_1)

	Control T_0 ($N = 19$)	MFS T_0 ($N = 19$)	*P* value	MFS T_1 ($N = 19$)	*P* value
Indexed LA (mm/m²)	16.9 ± 1.9	16.8 ± 2.6	0.95	16.5 ± 2.6	0.71
LVEDD (mm)	48.5 ± 3.6	50.5 ± 6.6	0.86	51.1 ± 5.6	0.35
LVESD (mm)	30.2 ± 2.7	32.8 ± 6.1	0.42	33.2 ± 4.9	0.67
LVEF (%)	63.8 ± 10.0	64.1 ± 6.7	0.98	64.0 ± 5.8	0.84
Sm (cm/s)	9.6 ± 1.3	7.7 ± 1.3	<0.001	7.7 ± 1.1	0.94
E (cm/s)	88.1 ± 12.8	74.1 ± 14.2	0.006	72.9 ± 19.3	0.73
A (cm/s)	59.3 ± 14.5	51.8 ± 11.1	0.15	49.3 ± 15.3	0.34
E/A	1.5 ± 0.3	1.6 ± 0.6	0.84	1.6 ± 0.6	0.89
DT (ms)	135.6 ± 36.0	171.6 ± 37.1	0.002	184.3 ± 44.9	0.97
E_m (cm/s)	12.6 ± 3.3	9.0 ± 2.4	0.001	9.0 ± 2.4	0.99
E/E_m	7.3 ± 1.5	8.8 ± 2.8	0.07	8.6 ± 2.9	0.84

The fourth column presents *P* values for differences between controls and MFS patients at baseline (T_0), the sixth column presents *P* values for differences between MFS patients at baseline and at the end of follow-up (T_1).
DT, deceleration time; FS, fractional shortening; LA, left atrium; LVEDD, left ventricular end diastolic diameter; LVESD, left ventricular end systolic diameter; LVEF, left ventricular ejection fraction; MFS, Marfan syndrome.

without hemodynamic repercussion on the LV. Four patients underwent elective valve sparing aortic root replacement (all David procedure—mean age 31 (13.5) years) during follow-up.

Ex-vivo studies of the myocardium of WT and *Fbn1*$^{C1039G/+}$ mice

LV dysfunction in Fbn1*$^{C1039G/+}$ *mice is not associated with LV dilatation or fibrosis. Macroscopic and histological data demonstrate the absence of cardiomegaly (no ventricular dilatation, normal LV wall thickness, and no cardiomyocyte hypertrophy). *Bnp* was not differentially expressed between *Fbn1*$^{C1039G/+}$ and WT mice ($P = 0.43$), which concurs with the absence of LV dilatation and myocardial stretch in *Fbn1*$^{C1039G/+}$ mice (21). Staining with Picrosirius red did not reveal fibrosis in the myocardium of MFS mice (**Figure 2**). Expression analysis of *Col1a1* and *Col3a1*, the predominant interstitial collagens in the myocardium (22), were performed using real-time quantitative polymerase chain reaction. No significant differences in expression levels were observed between *Fbn1*$^{C1039G/+}$ and WT mice ($P > 0.05$; **Figure 2**).

Deterioration of LV function is associated with microfibril disruption. The distribution of fibrillin-1 and fibrillin-2, major constituents of microfibrils, in the mouse myocardium was evaluated by immunohistochemistry. In WT mice, fibrillin-1-positive microfibrils were expressed throughout the myocardium, whereas substantial reduction in the staining pattern of fibrillin-1 was observed in the myocardium of *Fbn1*$^{C1039G/+}$ mice (**Figure 3**). These abnormalities were a consistent feature in the myocardium of *Fbn1*$^{C1039G/+}$ mice. Interestingly, the observed abnormalities were not present in young *Fbn1*$^{C1039G/+}$ mice of 6 wk of age, not yet expressing a clinical cardiovascular phenotype. Fluorescent staining with a fibrillin-2 antibody showed similar changes in the staining pattern, i.e., fibrillin-2 being more expressed in WT and 6-wk-old *Fbn1*$^{C1039G/+}$ mice compared to 14-mo-old *Fbn1*$^{C1039G/+}$ mice (**Figure 3**).

Canonical and noncanonical TGFβ signaling is upregulated in MFS-related CMP. To investigate canonical (SMAD2/3) and noncanonical (ERK1/2 and JNK) TGFβ signaling in the myocardium, we performed western-blot analysis on myocardial tissue of 14-mo-old *Fbn1*$^{C1039G/+}$ and WT mice. Compared to WT littermates, *Fbn1*$^{C1039G/+}$ mice showed a significantly increased activation of SMAD2 and ERK1/2 (indicated as pSmad2 and pERK1/2, respectively) (**Figure 4**). pSMAD2 and pERK1/2 signaling levels showed a two- to threefold increase in the *Fbn1*$^{C1039G/+}$ mice ($P < 0.05$ for both). We found no upregulation of pJNK in the myocardium of *Fbn1*$^{C1039G/+}$ mice (data not shown).

LV dysfunction in the Fbn1C1039G/+ mouse myocardium is not mediated through altered integrin signaling. We sought to investigate whether the microfibril alterations were associated with abnormal signaling through the integrin pathway. To this aim, we performed western blotting of β1, α5, and α9 integrin. β1 integrin is the primary β integrin subunit expressed in the myocardium and has previously been linked to the development of dilated CMP (16–18) and α5 and α9 integrin directly bind to fibrillin-1 ((23,24), personal communication, Prof. L. Sakai). β1, α5, and α9 integrins were not differentially expressed ($P = 0.73$–0.91) (**Figure 5**). In order to investigate alterations in downstream integrin signaling, we performed western blot analysis of Focal Adhesion Kinase (FAK) and its phosphorylated form (pFAK). FAK is one of the first kinase molecules recruited into the focal adhesion complex, which is essential for initiation of intracellular signaling through integrin receptors. No significant differences in integrin signaling through FAK were found ($P = 1.0$) (**Figure 5**).

MMP2 and -9 expression is not upregulated in the Fbn1*$^{C1039G/+}$ *mouse myocardium. Matrix metalloproteinases (MMP)-2 and -9 upregulation is implicated in thoracic aortic aneurysm formation in MFS (25–27) as well as in the development of dilated CMP (28). In this view, they may be possible pathogenic substrates for MFS-related CMP. However, WB analysis of MMP2 and -9 did not demonstrate significant differences in protein expression between WT and *Fbn1*$^{C1039G/+}$ mice (**Supplementary Figure S2** online).

DISCUSSION

Over recent years, several independent studies demonstrated the presence of mild intrinsic left ventricular systolic and diastolic dysfunction in children and adult patients with MFS (3,4). More severe presentations of ventricular dysfunction requiring cardiac transplantation are rare, but have also been reported (29).

The underlying mechanism of MFS-related CMP is not elucidated, but since secondary causes such as valvular disease were

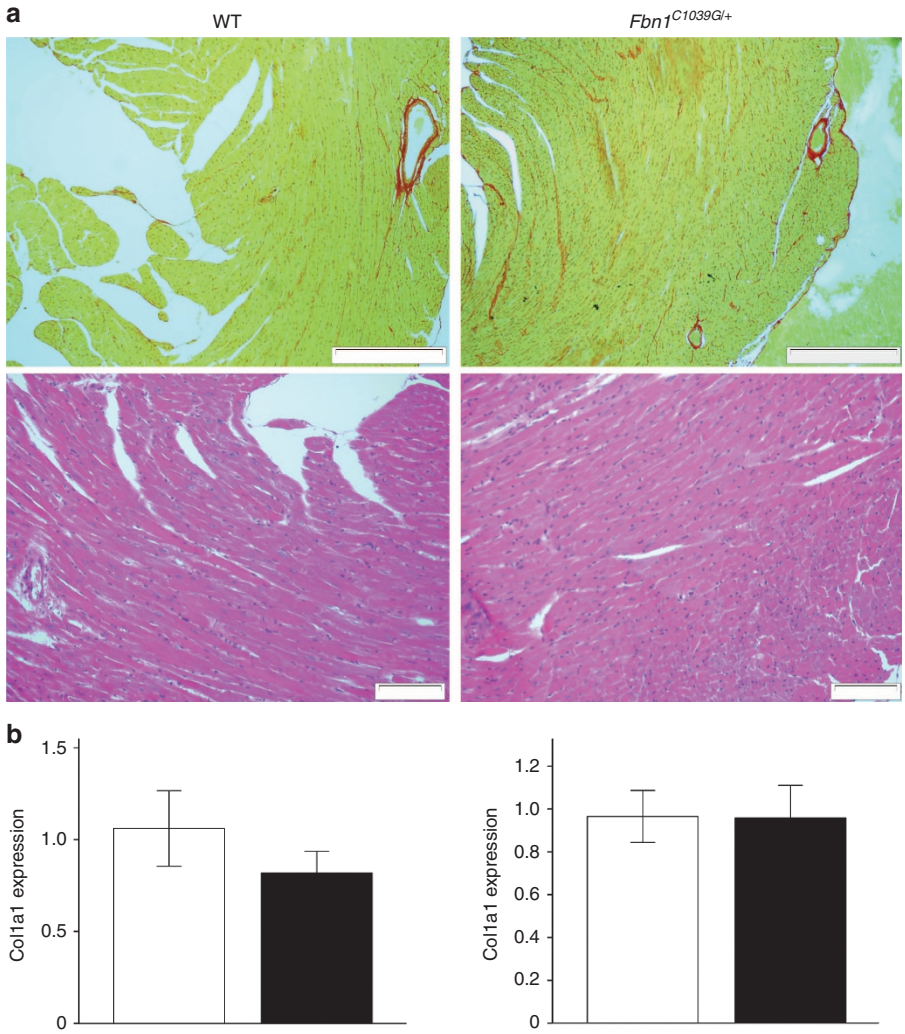

Figure 2. Role of fibrosis in Marfan syndrome-related cardiomyopathy. (**a**) Representative images of Picrosirius red and Hematoxylin-eosin staining of myocardium of wild-type (WT) and *Fbn1*$^{C1039G/+}$ mice. We observed no significant differences between WT and *Fbn1*$^{C1039G/+}$ mice. (**b**) Bar charts with error bars (representing 1 standard error) representing *Col1a1* and *Col3a1* mRNA expression in the mouse myocardium. The white bar represents WT mice and the black bar *Fbn1*$^{C1039G/+}$ mice. No significant differences in expression between WT ($N = 9$) and *Fbn1*$^{C1039G/+}$ ($N = 7$) mice were observed ($P > 0.05$ for all). Scale bars upper panels 500 µm, lower panels 100 µm.

excluded in all series of mild subclinical CMP (**Supplementary Figure S1** online), it is conceivable that the mutated *FBN1* gene lies at the basis of the myocardial dysfunction.

In order to explore the effect of mutated *FBN1* in the myocardium, we studied a representative and well-characterized murine MFS model, the *Fbn1*$^{C1039G/+}$ mouse model. This model represents a milder phenotype than the *Fbn1*$^{mgR/mgR}$, in which early onset dilated CMP has recently been evidenced (11). Since both mild and severe CMP phenotypes exist in humans, both mouse models may be complementary for pathogenic studies.

We confirmed the presence of mild LV dysfunction in the *Fbn1*$^{C1039G/+}$ model, which is in accordance with what is observed in the majority of MFS patients. Decreased LV function was not correlated with valvular dysfunction confirming the existence of a primary CMP in MFS. LV dysfunction remained mild and stable in adult mice, which is in line with preliminary human follow-up data from our center and with previously published follow-up results of MFS patients (30,31). In contrast to the first report on phenotypic characterization of the *Fbn1*$^{C1039G/+}$ model in which none of the mutant mice suffered from aortic dissection during a 2-y follow-up period (32), we demonstrate that *Fbn1*$^{C1039G/+}$ mice may suffer from (late onset) aortic dissection. Two *Fbn1*$^{C1039G/+}$ mice presented aortic dissection around 12 mo of age and one shortly thereafter. Chung *et al.* (33) reported aortic dissection in 5% of *Fbn1*$^{C1039G/+}$ mice between 5 and 8 mo of age. Collectively, these results indicate that aortic dissection is an infrequent and late-onset complication in the *Fbn1*$^{C1039G/+}$ model. Other MFS mouse models show more severe aortic phenotypes, as the *Fbn1*$^{mgR/mgR}$ model, which has a mean survival of 3.8 mo (34).

Since MFS is caused by mutations in the fibrillin-1 gene (*FBN1*) encoding the fibrillin-1 protein, a major constituent of microfibrils, the search for the explanation for the observed myocardial dysfunction was initiated at the level of structure and function of fibrillin-1 microfibrils in the myocardium of

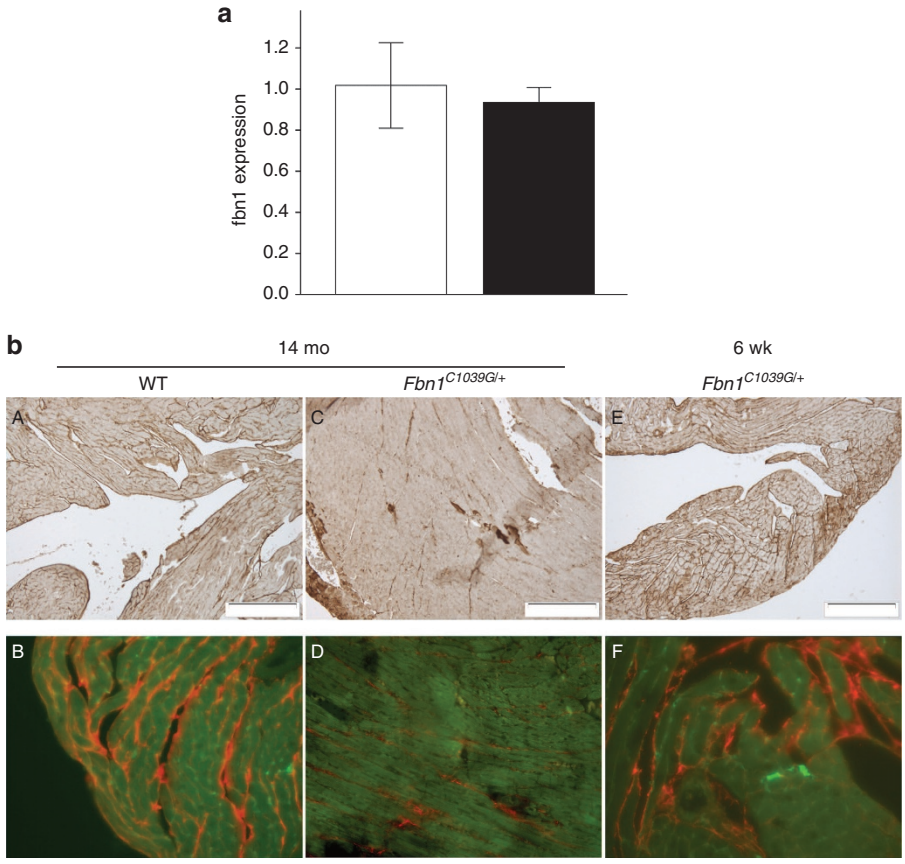

Figure 3. Fibrillin-1 expression in the myocardium of *Fbn1*$^{C1039G/+}$ and wild-type (WT) mice. (**a**) Bar chart with error bars (representing 1 standard error) representing *Fbn1* mRNA expression in the mouse myocardium. The white bar represents WT mice and the black bar represents *Fbn1*$^{C1039G/+}$ mice. No significant differences in expression between WT ($N = 9$) and *Fbn1*$^{C1039G/+}$ mice ($N = 7$) was observed ($P > 0.05$). (**b**) Representative images of immunohistological staining of fibrillin-1 in myocardium of 14-mo-old WT (panel **a**) and *Fbn1*$^{C1039G/+}$ (panel **c**) and 6-wk-old *Fbn1*$^{C1039G/+}$ (panel **e**) mice. Scale bars 200 µm. Representative images of immunofluorescent costaining of fibrillin-1 (red) and fibrillin-2 (green) in myocardium of 14-mo-old WT (panel **b**) and *Fbn1*$^{C1039G/+}$ (panel **d**) and 6-wk-old *Fbn1*$^{C1039G/+}$ (panel **f**) mice. Fourteen-month-old *Fbn1*$^{C1039G/+}$ mice showed substantial reduction in the staining pattern of fibrillin-1 and fibrillin-2 compared to WT and to *Fbn1*$^{C1039G/+}$ mice of 6 wk of age.

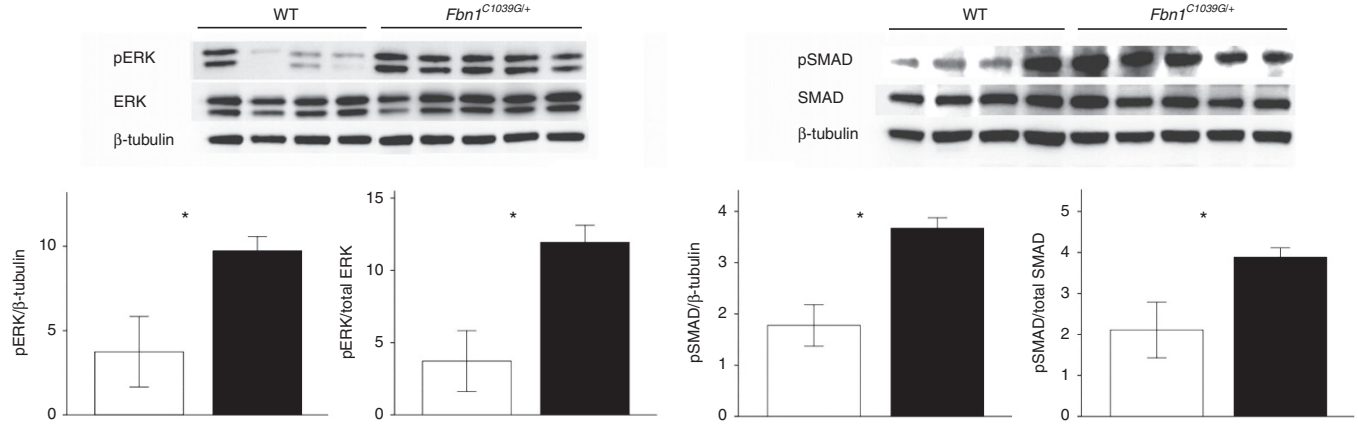

Figure 4. Canonical and noncanonical TGFβ signaling in the myocardium of four wild-type (WT) and five *Fbn1*$^{C1039G/+}$ mice. The figure shows representative results of western blots performed on myocardial extracts of all seven *Fbn1*$^{C1039G/+}$ and nine WT mice. The bar charts with error bars (representing 1 standard error) show normalization to β-tubulin and to the respective total proteins SMAD2 and ERK1/2. White bars represent WT mice and black bars represent *Fbn1*$^{C1039G/+}$ mice. pSMAD2 and pERK1/2 signaling levels showed a two- to threefold increase in the *Fbn1*$^{C1039G/+}$ mice. *P value < 0.05.

the *Fbn1*$^{C1039G/+}$ mouse model. Previous studies demonstrated that fibrillin-1 microfibrils contribute to the mechanical stability and elasticity of several tissues, such as the skin, eyes, and arterial system (12,13). We sought to investigate whether they are implicated in the mechanical properties of the myocardium as well.

We observed a normal expression of *Fbn1* mRNA in myocardial tissue of *Fbn1*$^{C1039G/+}$ mice, which is in agreement with

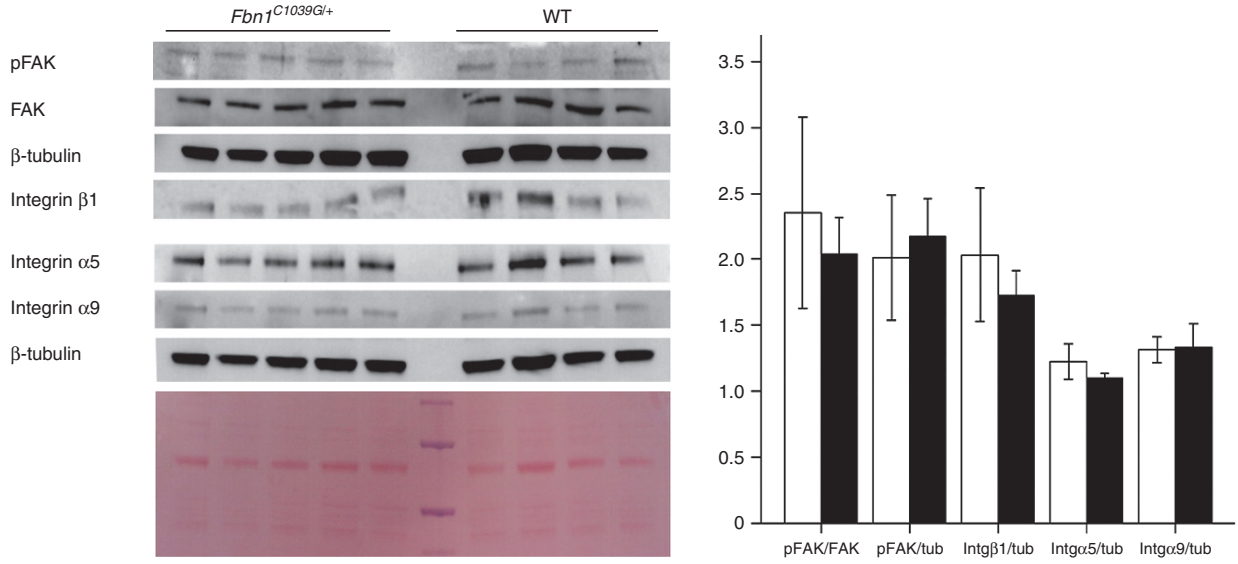

Figure 5. Integrin signaling. The figure shows representative results of western blots of pFAK, FAK, integrin β1, α5, and α9 performed on myocardial extracts of all seven *Fbn1*$^{C1039G/+}$ and nine wild-type (WT) mice. The bar charts with error bars (representing 1 standard error) show normalization to FAK and β-tubulin. White bars represent WT mice and black bars represent *Fbn1*$^{C1039G/+}$ mice. Ponceau staining is shown below the immunoblots as an indication of total protein loading. No significant differences in expression between WT and heterozygous mice were observed ($P > 0.05$ for all).

dermal findings in these mice (32). The mechanism by which *FBN1* mutations ultimately lead to perturbations of the microfibrillar network in the ECM is still a matter of debate. Two mechanisms have been suggested, (i) haploinsufficiency for WT fibrillin-1, implying that loss of normal fibrillin-1 deposition in the ECM below a certain threshold leads to subsequent impairment of microfibrillar assembly (32) and (ii) a dominant negative effect in which mutant fibrillin-1 monomers are incorporated in microfibrils, leading to microfibril destabilization followed by proteolytic degradation of aberrant microfibrils (35,36). In favor of a dominant negative effect, we noticed that 14-mo-old *Fbn1*$^{C1039G/+}$ mice with established LV dysfunction demonstrated less staining of fibrillin-1 compared to young mice, in whom no cardiac phenotype was present yet. Similarly, staining of fibrillin-2, which is another major component of microfibrils, was reduced in the adult *Fbn1*$^{C1039G/+}$ mice compared to WT mice. The observation that LV dysfunction coincides with a reduction of microfibrillar staining supports the hypothesis that microfibrils are required to maintain a normal myocardial function. Our findings are in accordance with the recently published results obtained in mice with cardiomyocyte-specific Fbn1 hypomorphism (*Fbn1*$^{\alpha MHC-/-}$ mouse model), in which myocardial dysfunction—in the absence of aortic disease—is related to a substantial reduction in fibrillin-1 (11).

In a next stage, we aimed to explore whether a defective ECM may alter TGFβ and integrin signaling.

Analogous to the results obtained in aortic tissue of the *Fbn1*$^{C1039G/+}$ mouse model (37,38), both canonical and noncanonical TGFβ signaling pathways are upregulated in the myocardium of the *Fbn1*$^{C1039G/+}$ mouse model, as evidenced by a significant increase of the active forms of SMAD2 and ERK1/2, respectively. This upregulation of TGFβ signaling was not associated with cardiac fibrosis. Absence of fibrosis has also been evidenced in humans where cardiac MRI in MFS patients did not reveal delayed enhancement, which is used as a marker of interstitial fibrosis (personal communication, Prof. Y. von Kodolitsch). Also MMP2 and -9, downstream products of TGFβ (26), are not involved in the development of CMP in the *Fbn1*$^{C1039G/+}$ mouse model. The question remains whether upregulation of the TGFβ pathway is independently involved in the development of MFS-related CMP or whether increased TGFβ signaling should be regarded as the result of a more complex final common pathway. In the *Fbn1*$^{mgR/mgR}$ mouse myocardium, selective upregulation of the noncanonical signaling pathway was evidenced. Early treatment with a TGFβ neutralizing antibody considerably reduced pERK levels, but did not rescue the cardiac phenotype. Consequently, the authors stated that altered TGFβ signaling plays no prominent role in the pathogenesis of CMP (11). However, it needs to be taken into account that the *Fbn1*$^{mgR/mgR}$ model is a severe model of MFS and other pathophysiological substrates may be implicated in the ultimate phenotype of each specific mouse model.

As fibrillin-1 microfibrils interact with integrin receptors, microfibrillar alterations might disturb mechanosignaling through the integrin pathway leading to reduced cardiomyocyte contractility (39). In the *Fbn1*$^{C1039G/+}$ myocardium, microfibril disintegration was not associated with defective integrin signaling as indicated by the absence of dysregulation of integrin subunits β1, α5, or α9 or of the downstream effector pFAK. In the *Fbn1*$^{mgR/mgR}$ mouse model, the expression of β1 integrin was also normal, but in contrast to our results pFAK was downregulated. This abnormal mechanosignaling was suggested to be due to an interaction between the angiotensin II type I receptor (AT1R) and the integrin pathway in response to mechanical stretch (11). The *Fbn1*$^{mgR/mgR}$ mouse model demonstrates severe mitral and aortic regurgitation

with LV dilatation. This mechanical stretch imposed on the LV can induce the AT1R in a ligand-independent manner leading to cardiomyocyte hypertrophy (16,40). In accordance with these findings, cardiomyocyte hypertrophy was evidenced in the *Fbn1*$^{mgR/mgR}$ mouse model (11). The *Fbn1*$^{C1039G/+}$ mice demonstrated LV dysfunction in the absence of obvious signs of mechanical stretch on the LV (normal end-diastolic LV dimensions and no cardiomyocyte hypertrophy), this might explain why pFAK is not altered in this model.

Conclusion

Our findings suggest that MFS-related CMP in the *Fbn1*$^{C1039G/+}$ model is associated with a deficient ECM and is not evoked by valvular dysfunction. As a consequence, microfibrils should be considered as important extracellular regulators of myocardial function. In the *Fbn1*$^{C1039G/+}$ model, CMP is subclinical, which is in accordance with most MFS patients. This renders the *Fbn1*$^{C1039G/+}$ model an interesting model to investigate the pathophysiology of MFS-related CMP. More severe human cardiac phenotypes also occur and are reflected by the findings in the previously reported *Fbn1*$^{mgR/mgR}$ mouse model. Further research is necessary to define what drives the severity and to address the pathophysiological relation between *FBN1* mutations, microfibrillar destabilization, and ventricular dysfunction and to explore the contribution of TGFβ in this process.

Limitations

We noticed variation in protein expression in the C57Bl6 mice. The results of repeated experiments were reproducible and environmental variation was excluded (all animals were kept in the same environment from breeding through testing). In our opinion, the differential protein expression is related to variation within the C57bl6 mice.

Due to underlying thoracic deformities adequate apical 2- and 3-chamber views, to assess LV volumes, were difficult to obtain in all patients (41). Therefore, LVEF based on LV diameters was computed. We assessed follow-up data of a small group of MFS patients, which may decrease statistical power. Additional prospective studies in larger patient groups combining both imaging studies and biomarker analyses are necessary to draw definite conclusions about the long-term evolution of CMP in MFS.

METHODS

Fbn1$^{C1039G/+}$ Mice

Mice heterozygous for a missense mutation in *Fbn1* (*Fbn1*$^{C1039G/+}$) were used for the study of the pathophysiology of LV dysfunction. The *Fbn1*$^{C1039G/+}$ line was maintained on a C57BL/6 background, allowing for valid comparisons. In order to avoid temporal- or background-specific variation, all comparisons were made between contemporary littermates. There were no significant differences in baseline characteristics (**Table 1**).

The Animal Experiments Were Approved by the Local Ethical Committee and Were Conducted in Compliance With the European Parliament Directive 2010/63/EU

Echocardiography

We performed serial ultrasound imaging of 11 *Fbn1*$^{C1039G/+}$ (six females) and nine WT (four females) mice at 1, 3, and 6 mo and in nine *Fbn1*$^{C1039G/+}$ (six females) and nine WT (four females) mice at 12 mo of age (two MFS mice had died of aortic dissection between the last two scans). A dedicated ultrasound apparatus (Vevo 2100, Visualsonics, Toronto, Canada), equipped with a high-frequency linear array transducer (MS 550D, frequency 22–55 MHz), was used. Recorded images were analyzed offline by two independent researchers (L.C. and J.D.B.) blinded to the genotype. The interobserver variability for the main measurements is given in **Supplementary Table S1** online. Detailed materials and methods for echocardiographic measurements are provided in the **Supplementary Material** online.

Western Blot Analysis, Histology, and Immunohistochemistry

All surviving animals (seven *Fbn1*$^{C1039G/+}$ and nine WT mice) were sacrificed at 14 mo of age for subsequent *ex-vivo* studies. Additionally, two WT and two *Fbn1*$^{C1039G/+}$ mice of 6 wk of age were sacrificed for immunohistochemical staining with anti-fibrillin-1 (pAb 9543) and anti-fibrillin-2 (pAb 0868) (both a gift from Prof. Lynn Sakai). Detailed materials and methods for western blot, quantitative polymerase chain reaction analyses, and histology are provided in the **Supplementary Material** online.

Clinical Studies

In order to correlate evolutionary findings obtained in MFS mice to the human MFS-related CMP phenotype, we analyzed serial ultrasound images, collected during the past 6 ± 1.9 y (range 3.4–10.3 y), of 19 MFS patients, previously reported by our group (20). In this previous study, we evidenced mild systolic and diastolic LV dysfunction as a primary manifestation of MFS. Demographic data are provided in **Supplementary Table S2** online. Digitized ultrasound scans obtained at baseline from our previous study (20) were reassessed and all measurements of baseline scans and follow-up scans were performed by L.C. and J.D.B. The interobserver variability for the main measurements is given in **Supplementary Table S3** online. Detailed materials and methods for echocardiographic measurements are provided in the **Supplementary Material** online. The study was approved by the local ethical committee and informed consent was obtained from all patients. This study conforms to the principles outlined in the Declaration of Helsinki and its later amendments.

Statistical Analysis

Results are presented as mean ± standard deviation. Follow-up echocardiographic data were analyzed with paired sample *t*-test for normal-distributed continuous variables; non-normal distributed values were compared using Wilcoxon Signed Rank test; χ^2 test was used to compare categorical variables. If not all cells had an expected count of 5 or more, Fisher's Exact test was applied. Data were analyzed with the unpaired sample *t*-test for normal-distributed continuous variables; non-normal distributed variables were compared using the Mann-Whitney *U*-test. A P value of < 0.05 was used to define statistical significance (two-sided). Univariate, and when appropriate, multivariate analysis and regression analysis for repeated measurements, were applied to assess the interaction between different parameters. Confounding factors were included in a multivariate model using the stepwise method, with entry and removal criteria set at $P < 0.1$. SPSS version 20.0 was used for the statistical analysis (SPSS, Chicago, IL).

SUPPLEMENTARY MATERIAL

Supplementary material is linked to the online version of the paper at http://www.nature.com/pr

ACKNOWLEDGMENTS

The authors wish to thank Petra Vermassen and Eveline Debals for their assistance in the lab.

STATEMENT OF FINANCIAL SUPPORT

J.D.B. is a Senior Clinical Researcher supported by the Flanders Research Fund. A.D.P. is holder of a Methusalem Grant (01M01108) from the Ghent University Special Research Fund. This study is supported by a donation of the Canadian Marfan Association, the Ghent University Special Research Fund (BOF10/GOA005) and the Hercules Foundation, Brussels, Belgium.

Disclosure: None to declare.

REFERENCES

1. Loeys BL, Dietz HC, Braverman AC, et al. The revised Ghent nosology for the Marfan syndrome. J Med Genet 2010;47:476–85.
2. Gray JR, Davies SJ. Marfan syndrome. J Med Genet 1996;33:403–8.
3. de Witte P, Aalberts JJ, Radonic T, et al. Intrinsic biventricular dysfunction in Marfan syndrome. Heart 2011;97:2063–8.
4. Angtuaco MJ, Vyas HV, Malik S, Holleman BN, Gossett JM, Sachdeva R. Early detection of cardiac dysfunction by strain and strain rate imaging in children and young adults with marfan syndrome. J Ultrasound Med 2012;31:1609–16.
5. Dietz HC. TGF-beta in the pathogenesis and prevention of disease: a matter of aneurysmic proportions. J Clin Invest 2010;120:403–7.
6. Tamargo J. TGFβ3 mutations cause arrhythmogenic right ventricular dysplasia type 1 and open the door to understanding the biological role of TGFβ3 (where there's a will, there's a way). Cardiovasc Res 2012;96:188–90; discussion 191–4.
7. Pauschinger M, Knopf D, Petschauer S, et al. Dilated cardiomyopathy is associated with significant changes in collagen type I/III ratio. Circulation 1999;99:2750–6.
8. Khan R, Sheppard R. Fibrosis in heart disease: understanding the role of transforming growth factor-beta in cardiomyopathy, valvular disease and arrhythmia. Immunology 2006;118:10–24.
9. Li RK, Li G, Mickle DA, et al. Overexpression of transforming growth factor-beta1 and insulin-like growth factor-I in patients with idiopathic hypertrophic cardiomyopathy. Circulation 1997;96:874–81.
10. Wu W, Muchir A, Shan J, Bonne G, Worman HJ. Mitogen-activated protein kinase inhibitors improve heart function and prevent fibrosis in cardiomyopathy caused by mutation in lamin A/C gene. Circulation 2011;123:53–61.
11. Cook JR, Carta L, Bénard L, et al.; GenTAC Registry Consortium. Abnormal muscle mechanosignaling triggers cardiomyopathy in mice with Marfan syndrome. J Clin Invest 2014;124:1329–39.
12. Ramirez F, Dietz HC. Fibrillin-rich microfibrils: Structural determinants of morphogenetic and homeostatic events. J Cell Physiol 2007;213:326–30.
13. Kielty CM, Wess TJ, Haston L, Ashworth JL, Sherratt MJ, Shuttleworth CA. Fibrillin-rich microfibrils: elastic biopolymers of the extracellular matrix. J Muscle Res Cell Motil 2002;23:581–96.
14. Parker KK, Ingber DE. Extracellular matrix, mechanotransduction and structural hierarchies in heart tissue engineering. Philos Trans R Soc Lond B Biol Sci 2007;362:1267–79.
15. Horiguchi M, Ota M, Rifkin DB. Matrix control of transforming growth factor-β function. J Biochem 2012;152:321–9.
16. Lal H, Verma SK, Foster DM, et al. Integrins and proximal signaling mechanisms in cardiovascular disease. Front Biosci (Landmark Ed) 2009;14:2307–34.
17. Hannigan GE, Coles JG, Dedhar S. Integrin-linked kinase at the heart of cardiac contractility, repair, and disease. Circ Res 2007;100:1408–14.
18. Shai SY, Harpf AE, Babbitt CJ, et al. Cardiac myocyte-specific excision of the beta1 integrin gene results in myocardial fibrosis and cardiac failure. Circ Res 2002;90:458–64.
19. Knöll R, Postel R, Wang J, et al. Laminin-alpha4 and integrin-linked kinase mutations cause human cardiomyopathy via simultaneous defects in cardiomyocytes and endothelial cells. Circulation 2007;116:515–25.
20. De Backer JF, Devos D, Segers P, et al. Primary impairment of left ventricular function in Marfan syndrome. Int J Cardiol 2006;112:353–8.
21. Luchner A, Muders F, Dietl O, et al. Differential expression of cardiac ANP and BNP in a rabbit model of progressive left ventricular dysfunction. Cardiovasc Res 2001;51:601–7.
22. Kassiri Z, Khokha R. Myocardial extra-cellular matrix and its regulation by metalloproteinases and their inhibitors. Thromb Haemost 2005;93:212–9.
23. Bax DV, Bernard SE, Lomas A, et al. Cell adhesion to fibrillin-1 molecules and microfibrils is mediated by alpha 5 beta 1 and alpha v beta 3 integrins. J Biol Chem 2003;278:34605–16.
24. Bax DV, Mahalingam Y, Cain S, et al. Cell adhesion to fibrillin-1: identification of an Arg-Gly-Asp-dependent synergy region and a heparin-binding site that regulates focal adhesion formation. J Cell Sci 2007;120(Pt 8):1383–92.
25. Chung AW, Yang HH, Radomski MW, van Breemen C. Long-term doxycycline is more effective than atenolol to prevent thoracic aortic aneurysm in marfan syndrome through the inhibition of matrix metalloproteinase-2 and -9. Circ Res 2008;102:e73–85.
26. Lindsay ME, Dietz HC. Lessons on the pathogenesis of aneurysm from heritable conditions. Nature 2011;473:308–16.
27. Xiong W, Meisinger T, Knispel R, Worth JM, Baxter BT. MMP-2 regulates Erk1/2 phosphorylation and aortic dilatation in Marfan syndrome. Circ Res 2012;110:e92–e101.
28. Polyakova V, Loeffler I, Hein S, et al. Fibrosis in endstage human heart failure: severe changes in collagen metabolism and MMP/TIMP profiles. Int J Cardiol 2011;151:18–33.
29. Knosalla C, Weng YG, Hammerschmidt R, et al. Orthotopic heart transplantation in patients with Marfan syndrome. Ann Thorac Surg 2007;83:1691–5.
30. Meijboom LJ, Timmermans J, van Tintelen JP, et al. Evaluation of left ventricular dimensions and function in Marfan's syndrome without significant valvular regurgitation. Am J Cardiol 2005;95:795–7.
31. Scherptong RW, Vliegen HW, van der Wall EE, et al. Biventricular performance in patients with marfan syndrome without significant valvular disease: comparison to normal subjects and longitudinal follow-up. J Am Soc Echocardiogr 2011;24:1392–1399.e1.
32. Judge DP, Biery NJ, Keene DR, et al. Evidence for a critical contribution of haploinsufficiency in the complex pathogenesis of Marfan syndrome. J Clin Invest 2004;114:172–81.
33. Chung AW, Au Yeung K, Cortes SF, et al. Endothelial dysfunction and compromised eNOS/Akt signaling in the thoracic aorta during the progression of Marfan syndrome. Br J Pharmacol 2007;150:1075–83.
34. Pereira L, Lee SY, Gayraud B, et al. Pathogenetic sequence for aneurysm revealed in mice underexpressing fibrillin-1. Proc Natl Acad Sci USA 1999;96:3819–23.
35. Robinson PN, Godfrey M. The molecular genetics of Marfan syndrome and related microfibrillopathies. J Med Genet 2000;37:9–25.
36. Charbonneau NL, Carlson EJ, Tufa S, et al. *In vivo* studies of mutant fibrillin-1 microfibrils. J Biol Chem 2010;285:24943–55.
37. Habashi JP, Judge DP, Holm TM, et al. Losartan, an AT1 antagonist, prevents aortic aneurysm in a mouse model of Marfan syndrome. Science 2006;312:117–21.
38. Holm TM, Habashi JP, Doyle JJ, et al. Noncanonical TGFβ signaling contributes to aortic aneurysm progression in Marfan syndrome mice. Science 2011;332:358–61.
39. Harston RK, Kuppuswamy D. Integrins are the necessary links to hypertrophic growth in cardiomyocytes. J Signal Transduct 2011;2011:521742.
40. Zablocki D, Sadoshima J. Solving the cardiac hypertrophy riddle: The angiotensin II-mechanical stress connection. Circ Res 2013;113:1192–5.
41. Selamet Tierney ES, Levine JC, Chen S, et al.; Pediatric Heart Network Investigators. Echocardiographic methods, quality review, and measurement accuracy in a randomized multicenter clinical trial of Marfan syndrome. J Am Soc Echocardiogr 2013;26:657–66.